Supporting Information

Electrocatalytically Active Graphene-Porphyrin MOF Composite for Oxygen Reduction Reaction (ORR)

*Maryam Jahan, Qiaoliang Bao, Kian Ping Loh**

Department of Chemistry, National University of Singapore, 3 Science Drive 3, Singapore 117543.

* To whom correspondence should be addressed. Email: chmlohkp@nus.edu.sg

Supporting Information

S1. Experimental Section

S2. Summary of crystal and refinement data for $(Fe\text{-}P)_n$ MOF and $(G\text{-}dye\text{-}FeP)_n$ MOFs.

S3. Comparison between GO and $(G\text{-}dye\ 50\ wt\%\text{-}FeP)_n$ MOF electrodes

S4. Cyclic voltammograms of $(G\text{-}dye\ 50\ wt\ \%\ \text{-}FeP)_n$ MOF and Pt nanoparticles in KOH solution

S5. Stability and reproducibility of GO electrode

S6. Comparison of RDE results between $(G\text{-}dye\ 50wt\%\ \text{-}FeP)_n$ MOF and $(G\text{-}dye\ 65\ wt\%\ \text{-}FeP)_n$ MOF

S7. Comparison of durability of $(G\text{-}dye\ 50\ wt\ \%\ \text{-}FeP)_n$ MOF , Pt nanoparticles, and Ni Foam

S8. X-ray photoelectron spectroscopy of $(G\text{-}dye\ 10\ wt\%\text{-}FeP)_n$ MOF and $(Fe\text{-}P)_n$ MOF

S9. A linear relationship between absorbance and concentration in DMF

S10. TGA and DTA study

S11. Evidences to prove the presence of Graphene sheet inside the framework

S12. References

S1. Experimental Section

Reagents and Chemicals. All chemicals purchased were of the purest grade and used as received from Sigma-Aldrich unless otherwise stated.

Graphite Oxide (GO) and reduced GO sheets were prepared following the procedure reported in literature.[1]

4-(4-Nitrostyryl) pyridine: A mixture of 4-nitro benzaldehyde (3 g, 20 mmol) and 4-picoline (2.3 g, 25 mmol) in 15 mL acetic anhydride was refluxed over night for 12 h.[2] The cooled mixture was poured onto ice and neutralized with 40 % NaOH aqueous solution. Extraction was carried out with ethyl acetate and the organic layer was concentrated by rotary evaporator. The residue was recrystallized with EA/HEX=1/1 to give 2.0 g (9 mmol, 45 %) 4-(4-Nitrostyryl) pyridine.

4-(4-aminostyryl) pyridine : To a mixture of 4-(4-Nitro styryl) pyridine (2 g, 9 mmol) and Pd on activated carbon (10 %, 50 mg) in ethanol (100 mL) was added hydrazine monohydrate (2 mL).[3] The mixture was heated and refluxed for 2 hours and checked with thin layer chromatography. When the reaction is finished, the hot solution was filtered and the solvent was concentrated. The residue was recrystallized in ethanol to give 1.45 g (7.4 mmol, 82 %) 4-(4-aminostyryl) pyridine.

4-styrylpyridine - Functionalized Graphene (G-dye): **Solution A :** The 4-styrylpyridine diazonium solution was prepared by the following procedures: 343 mg of 4-(4-aminostyryl) pyridine (1.75 mmol) and 131.5 mg of sodium nitrite (1.89 mmol) were added to 40 mL water in ice bath.[4] This solution was added quickly to 3 mL HCl solution (10 %, 3.2 M, 9.6 mmol) and stirred for 45 min. The temperature was maintained at 0-5 ^{o}C during the reaction and the solution turned orange at the end. Solution A should be freshly prepared just before carrying out the experiment.

Solution B: the preparation of G-dye was performed by sonicating 150 mg of r-GO dispersed in 1 wt % aqueous sodium dodecylbenzensulfonate (SDBS) surfactant in 150 mL water.[5] The diazonium salt solution (solution A) was added quickly to the r-GO solution (solution B) in an ice bath under stirring and the mixture was maintained in ice bath at 0 - 5 ^{o}C for around 4 hours. Next, the reaction was stirred

at room temperature for another 4 hours. Finally, the solution was filtered using 0.2 μm polyamid membrane and washed several times with water, ethanol, DMF, and acetone.

$(Fe\text{-}P)_n$ MOF: The synthesis follows previous report with some modifications.[6] 5,10,15,20–Tetrakis (4-carboxyl) - 21H, 23H-porphine (TCPP) (0.05 mmol) and $FeCl_3$ (0.15 mmol) and 0.1 M HCl acid (1.2 mL, 0.12 mmol) in ethanol were dissolved in a mixture of 4 mL DMF and 8 mL ethanol. The final mixture was sealed in a small capped vial and sonicated to ensure homogeneity. The vial was heated at 150 °C in an oven for 48 h, followed by slow cooling to room temperature. The crystals were collected *via* filtration and washed with DMF and ethanol

$(G\text{-}dye\ \text{-}FeP)_n$ MOF: TCPP (0.05 mmol), $FeCl_3$ (0.15 mmol) and 0.1 M HCl acid (1.2 mL, 0.12 mmol) in ethanol were dissolved in a mixture of 4 mL DMF and 8 mL ethanol. Varying amounts of G-dye (5, 10, 25, and 50 wt %: based on the total mass of starting solid materials) were added to the mixtures. The final mixture was sealed in a small capped vial and sonicated to ensure homogeneity. The vial was heated at 150 °C in an oven for 48 hours, followed by slow cooling to room temperature. The crystals were collected *via* filtration and washed with DMF and ethanol.

Instrumentations

SEM images were recorded using the JEOL 6701 FESEM (field emission scanning electron microscopy) at 30 kV. FT-IR measurements were recorded at room temperature on the Varian 3100 FT-IR spectrometer. The samples were ground with KBr and then pressed into disks. AFM images were collected in the tapping mode using the SPM D3100 from Veeco and the specimens studied were coated freshly on silica substrates by spin-casting. UV-Vis spectroscopic data was collected using the UV-2450 Shimadzu UV-Vis Spectrometer with water as the solvent and a path length of 1 cm. N_2 adsorption-desorption isotherms were measured at –196 °C on an automatic volumetric sorption analyzer (Micromeritics, ASAP2020). Powder XRD diffraction was carried out using a Siemens D5005 X-ray diffractometer with CuKa line (l=1.54060 A^o) as the incident beam which is calibrated by SiO_2. A

Gobel mirror was employed as a monochromator. The sample powder was ground and then loaded into a glass holder and leveled with a glass slide before mounting it on the sample chamber. The specimens were scanned from 1.4 – 60^{o}. The scan step-width was set to 0.005^{o} and the scan rate to 0.005^{o} s^{-1}. XRD data analysis was performed using Reflex module in Materials Studio (Accelrys) software suites. Thermogravimetric analysis (TGA) and differential thermal analysis (DTA) were recorded by a Rigaku TG8101D and TAS 300 data-processing system with an aluminum pan under N_2 with a heating rate of 10 ^{o}C/min. The Raman spectra were carried out with a WITEC CRM200 Raman system. The excitation source is a 532 nm laser (2.33 eV) with laser power adjusted below 0.2 mW to avoid laser-induced local heating. X-ray photoelectron spectroscopy (XPS) spectra of catalyst were obtained using PHI Quantera instrument equipped with a Mg monochromatic X-ray source at a power of 350 W.

Voltammetric experiments were performed using Autolab PGSTAT30 digital potentiostat/ galvanostat. All the measurements were carried out in a polytetrafluoroethylene (PTFE) house (V = 5 mL) at room temperature using a three-electrode system with glassy carbon (GC) electrode as working electrode, Pt wire as counter electrode, and 1M KCl-Ag/AgCl as reference electrode. Cyclic voltammeters (CVs) were typically performed at a scan rate of 50 mV/s. All potentials were measured and reported using Ag/AgCl reference electrode. The cyclic voltammogram experiments were conducted in N_2 and O_2-saturated 0.1 M KOH solution for oxygen reduction reaction. RDE experiments were carried out on a RRDE-3A (ALS Co., Ltd) and the CH instruments electrochemical workstation (CH instrument, Inc. Austin) bipotentiostat. RDE measurements were performed in the oxygen-saturated 0.1 M KOH solution at rotation rates varying from 400 to 3500 rpm and with the scan rate of 10 mV/s. Linear sweep voltametry was performed at the RDE GCE glassy carbon disk electrode with a 4-mm diameter, Pt electrode, and Ag/AgCl reference electrode. Prior to use, the working electrode is polished mechanically with diamond down to alumina slurry to obtain a mirror-like surface and then washed with DI water and acetone and allowed to dry. 1 mg of each grinded sample was dispersed in 0.5 ml of Ethanol by sonication, respectively. 10.0 µl suspension of each catalyst was pipetted onto the glassy carbon electrode surface. The electrode was allowed to dry at room

temperature for 30 min in a desiccator before measurement. After drying, a catalyst loading of 159.2 $\mu g.cm^{-2}$ (the glass carbon electrode with a diameter of 4 mm) was obtained.

S2. Summary of crystal and refinement data for $(Fe\text{-}P)_n$ MOF and $(G\text{-}dye\text{-}FeP)_n$ MOF composites

XRD patterns were indexed using the program X-Cell in Materials Studio (Accelrys) software suites. In the composite, the MOF is the host material and G-dye or r-GO are just like impurities and may give some impurity reflection. X-Cell is specifically designed to deal with the presence of impurity peaks and offers the best chance of identifying the correct indexing solution if impurities are present. For all the three composites: (G-dye 5 wt % -FeP)$_n$ MOF, (G-dye 10 wt % -FeP)$_n$ MOF and evacuated (G-dye 10 wt % -FeP)$_n$ MOF, the impurity tolerance level is set to 1 to generate the best solution. The following table gives a summary of indexing and refinement data for $(Fe\text{-}P)_n$ MOF and (G-dye -FeP)$_n$ MOF composites.

Table S1. Lattice information of $(Fe\text{-}P)_n$ MOF, and (G-dye -FeP)$_n$ MOF composites

	$(Fe\text{-}P)_n$ MOF	(G-dye 5 wt % -FeP)$_n$ MOF	(G-dye 10 wt % -FeP)$_n$ MOF
Rel. FOM	0.345	0.139	0.115
FOM	658	238	182
Peaks Found	11 of 12	13 of 14	15 of 16
System	Triclinic	Monoclinic	Monoclinic
a	9.8117	20.3574	4.989
b	8.2878	5.2154	16.8836
c	4.976	11.9129	12.599
α	88.823	90	90
β	91.491	99.711	92.624
γ	101.272	90	90
Volume	396.65	1246.71	1060.13
Zero	-0.09518	0.0255	0.03519
Extinction Class	P-1	C2	P2/c
2theta Div	0.005455	0.021084	0.026762
Stability	2	1	3
Impurities	0	1	1
Out	29	33	33
Calc	40	49	51

Rel. FOM: is the relative figure of merit.

FOM: is the de Wolff figure of merit.

Peaks Found: indicates how many peaks defined for indexing were successfully indexed using this solution.

System: is the crystal system of the indexing solution.

Lattice parameters: a, b, c, α, β, γ

Volume: is the unit cell volume for the solution.

Zero: is the zero point correction.

Extinction class: is the representative space group of the indexing solution.

2theta div: is the average absolute difference between the experimental and calculated peak positions in degrees.

Stability: is the stability parameter for the solution. This parameter indicates, roughly, the minimum number of experimental peaks that need to be removed so that the indexing solution is no longer uniquely defined. The higher the stability parameter, the more reliable the solution. This parameter is only valid for 3D searches and is omitted if 1D or 2D searches are performed.

Impurities: indicates the number of impurity peaks.

Out: indicates the number of calculated peaks which have no overlap with observed reflections.

Calc: displays the total number of calculated peaks in the powder pattern between 0 and the maximum 2-theta of the input experimental data, given the unit cell and extinction class.

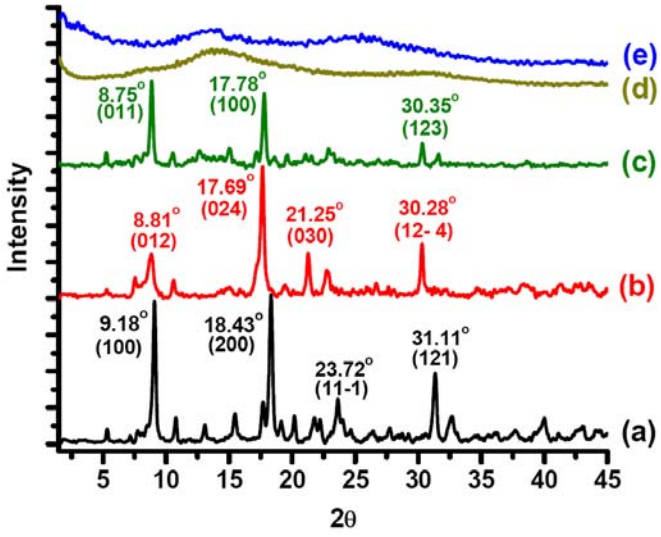

Figure S1. XRD pattern of (a) $(Fe\text{-}P)_n$ MOF, (b) (G-dye 5 wt % -$FeP)_n$ MOF, (c) (G-dye 10 wt % -$FeP)_n$ MOF, (d) (G-dye 25 wt % -$FeP)_n$ MOF [Note: similar to the XRD pattern of (G - dye 50 wt % -$FeP)_n$ MOF] , and (e) G-dye.

S3. Comparison between GO and (G-dye 50 wt%-FeP)$_n$ MOF electrodes

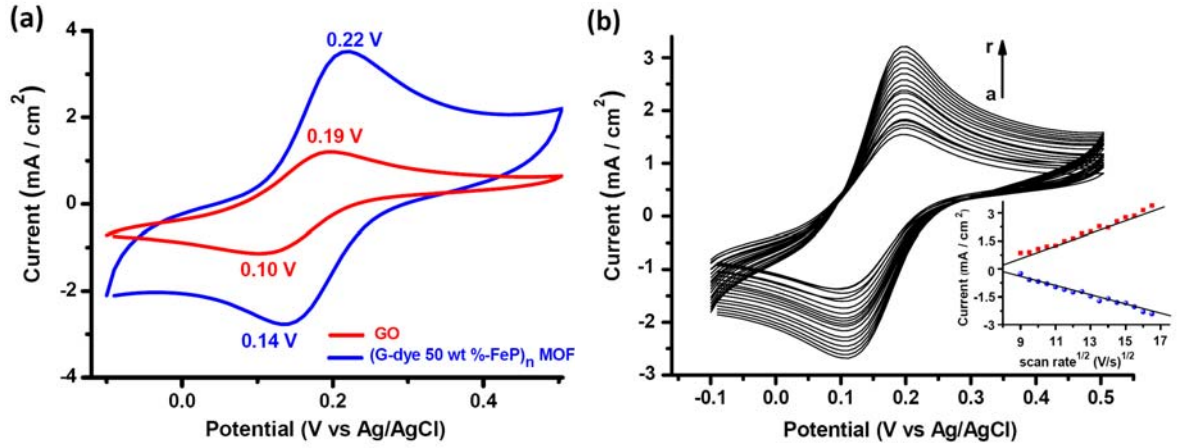

Figure S2. (a) Comparison of Cyclic voltammograms between GO [red curve] and (G-dye 50 wt % -FeP)$_n$ MOF [blue curve] in 10 mM $Fe(CN)_6^{3-/4-}$ /1 M KCl at scan rate of 50 mV/s. **(b)** Cyclic voltammograms of GO on GC electrode in 10 mM $Fe(CN)_6^{3-/4-}$ / 1 M KCl at various scan rates from 80 mV/s to 270 mV/s. Inset (i) : plot of peak current *vs.* (scan rate)$^{1/2}$ of GO drop casted on the GC electrode.

S4. Cyclic voltammograms of (G-dye 50 wt % -FeP)$_n$ MOF and Pt nanoparticles in KOH solution

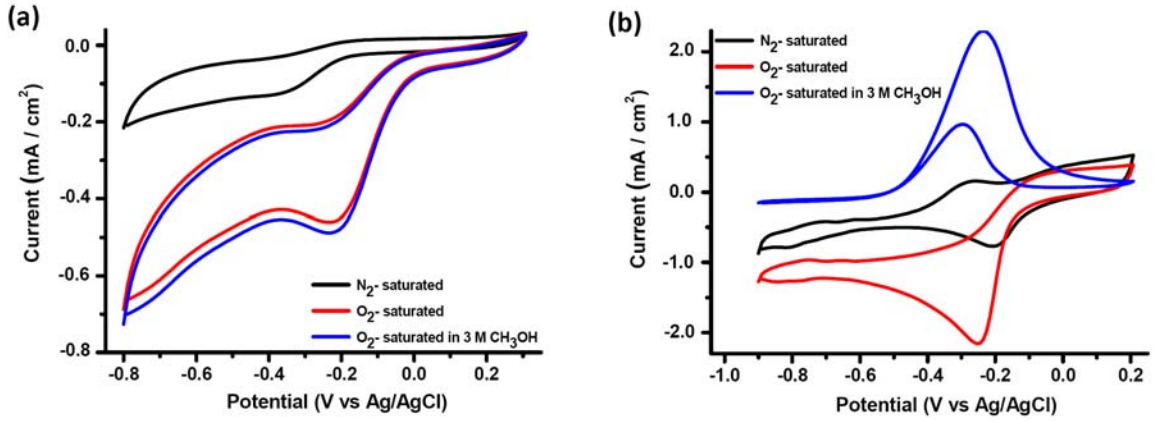

Figure S3. Cyclic voltammograms of **(a)** (G-dye 50 wt % -FeP)$_n$ MOF and **(b)** Pt nanoparticles ($NaPt(Cl)_6$. $6H_2O$ 10 mM / $NaSO_4$ 0.5 M) drop-casted on a GC electrode in various electrolyte system. These include N_2-saturated 0.1M solution of KOH , O_2-saturated 0.1M solution of KOH, and O_2-saturated 0.1M solution + 3 M CH_3OH (3M).

S5. Stability and reproducibility of GO electrode

The stability of the GO were investigated as an example among our samples by performing cyclic voltammograms of 50 repetitive cycles at scan rate of 50 mV/s in 0.1M KOH solution saturated with O_2. As shown in **Figure S4**, there were no changes in the peak potential, but decreasing in current density by increasing the number of cycle.

The reproducibility of GO was checked by immersing the GO electrode in the same solution for 24 h. CV was carried out again in O_2-saturated solution and compared with the initial CV obtained under the same conditions. The film of GO was found to be well reproducibility. Thus the stability and the reproducibility of the GO electrode used for electrocatalytic studies were established. The same results were seen for the other samples.

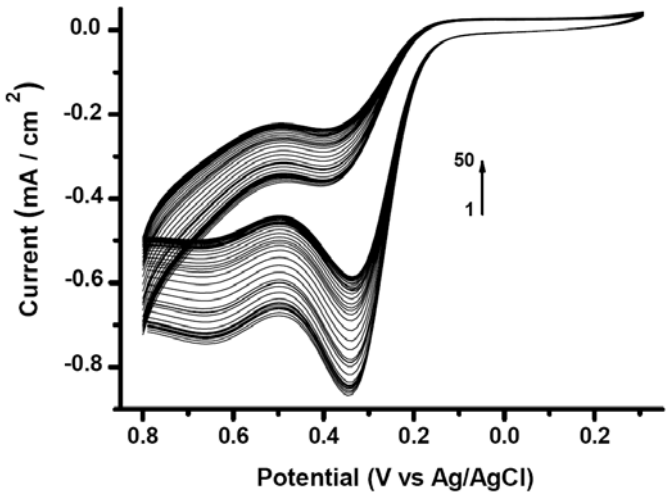

Figure S4. Cyclic voltammograms of GO in 10 mM $Fe(CN)_6^{3-/4-}$ /1 M KCl at scan rate of 50 mV/s after 50 cycles.

S6. Comparison of RDE results between (G-dye 50 wt% -FeP)$_n$ MOF and (G-dye 65 wt % -FeP)$_n$ MOF

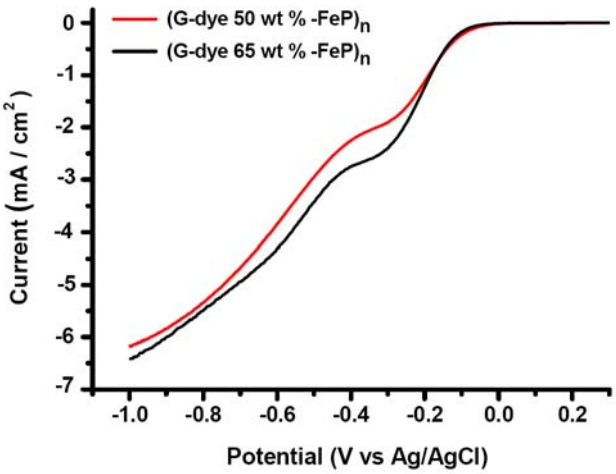

Figure S5. RDE voltammograms of (G-dye 50 wt % -FeP)$_n$ MOF and (G-dye 65 wt % -FeP)$_n$ MOF at a rotation rate of 2000 rpm.

S7. Comparison of durability of (G-dye 50 wt % -FeP)$_n$ MOF , Pt nanoparticles, and Ni Foam

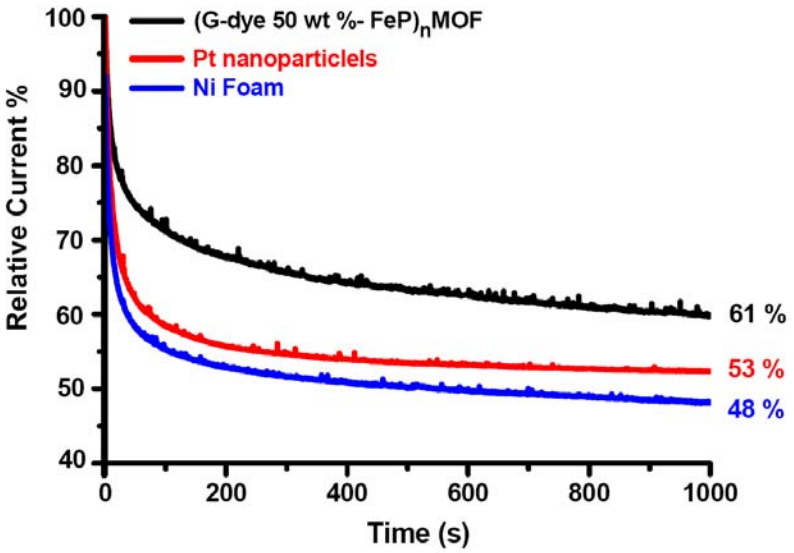

Figure S6. Current-time chronoamperometric responses of (G-dye 50 wt% -FeP)$_n$ MOF, Pt nanoparticles ($NaPt(Cl)_6$. $6H_2O$ 10 mM / $NaSO_4$ 0.5 M) , and Ni foam on a GC electrode at -0.23 V in O_2-saturated 0.1 M KOH. The percentages are reference to the initial current at time zero.

S8. X-ray photoelectron spectroscopy of (G-dye 10 wt%-FeP)$_n$ MOF and (Fe-P)$_n$ MOF

To study the chemical environment of the atoms in the compounds, X-ray photoelectron spectroscopy (XPS) was performed. **Figure S7** shows that there are two chemically shifted Fe peaks in the XPS spectra of both compounds. The peaks are assignable to the Fe inside the porphyrin core (connected to four electronegative nitrogen atoms from pyrrole groups) and the Fe connected to the two electronegative oxygen groups of two adjacent porphyrin sites, respectively. Accordingly, the electron deficiency of porphyrinic Fe is higher than the bridging Fe, giving rise to its higher binding energy. This gives rise to a higher binding energy for the porpyrinic iron and lower binding energy for the bridging iron. It can be seen that the binding energy of Fe $2p_{3/2}$ in (G-dye 10 wt % -FeP)$_n$ MOF is lower than that in (Fe -P)$_n$ MOF in **Figure S7(C).** This shift is attributed to the coordination of the pyridine ligand to iron in (G-dye 10 wt % -FeP)$_n$ MOF, which increases the electron density on the iron

(thus decreasing binding energy). **Figure S8 (A)** shows one peak for the N 1*s* of (Fe -P)$_n$ MOF assignable to the pyrrole nitrogen. Considering that there are two different nitrogen environment in (G-dye 10 wt % -FeP)$_n$ MOF arising from pyrrole groups located in the porphyrin core and pyridine groups from the dye, the two peaks at 398.7 and 400.6 eV are attributed to N 1*s* of pyridine N and pyrrole atoms[7,8] , respectively, as shown in **Figure S8(B)**.

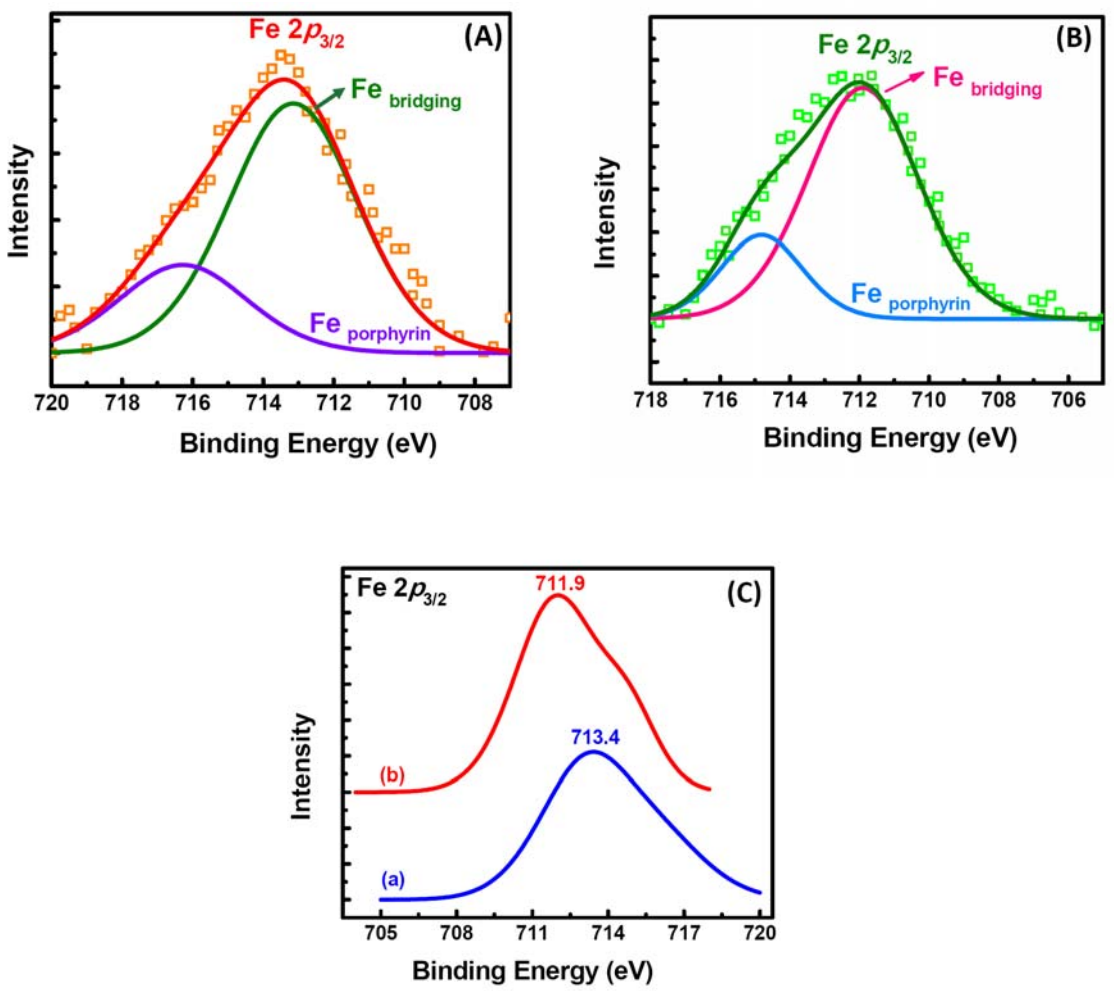

Figure S7. (A) The Fe 2$p_{3/2}$ core level spectra for (Fe-P)$_n$ MOF. **(B)** The Fe 2$p_{3/2}$ core level spectra for (G-dye 10 wt % -FeP)$_n$ MOF. **(C)** Comparison between The Fe 2$p_{3/2}$ core level spectra for (a) (Fe-P)$_n$ MOF , (b) (G-dye 10 wt % -FeP)$_n$ MOF.

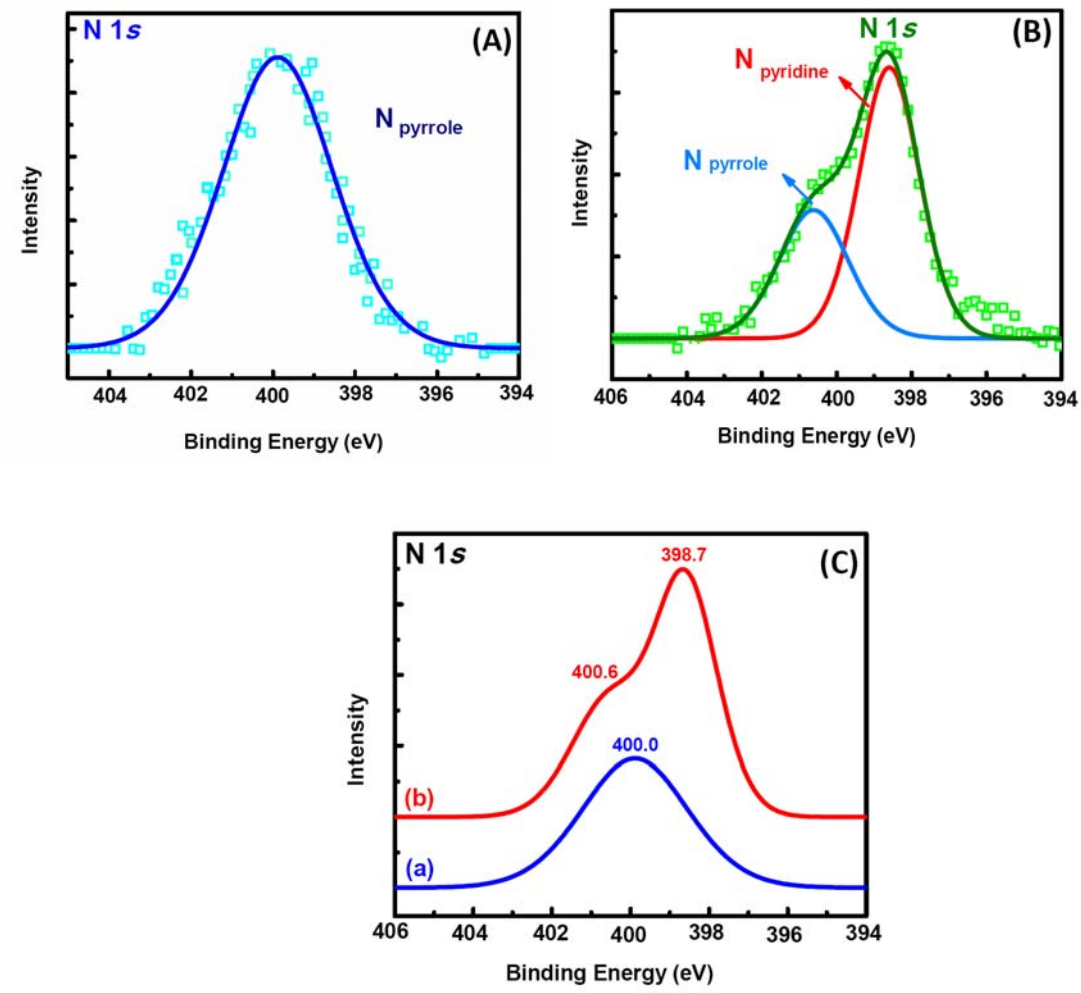

Figure S8. (A) The N 1*s* core level spectra for $(Fe\text{-}P)_n$ MOF. **(B)** The N 1*s* core level spectra for (G-dye 10 wt % -$FeP)_n$ MOF. **(C)** Comparison between The N 1*s* core level spectra for (a) $(Fe\text{-}P)_n$ MOF , (b) (G-dye 10 wt % -$FeP)_n$ MOF.

S9. A linear relationship between absorbance and concentration in DMF

This is indicative of good dispersion of G-dye because aggregation at high concentration will cause a deviation from linearity in the Beer's plot.[9]

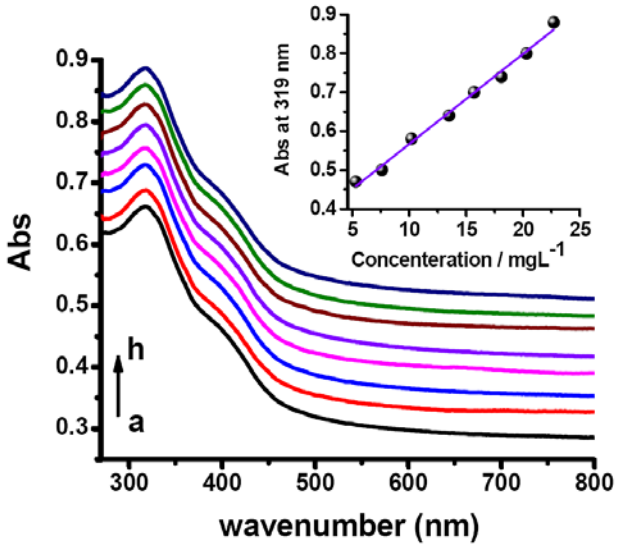

Figure S9. Concentration dependence of UV-vis absorption spectra of G-dye in DMF (concentration are 4.2, 6.6, 9.5, 11.4, 14.8, 16.5, 19.3, and 22.7 mg L^{-1}, from a-h, respectively). The insert shows the plot of optical density at 319 nm versus concentration. The straight lines are linear least-squares fit to the data, indicating G-dye was dissolved homogeneously in DMF.

S10. TGA and DTA study

To evaluate the thermal stability of the hybrid MOFs, TGA and DTA studies were performed. The results show that by increasing the amount of G-dye, the amount of residue left after thermal pyrolysis decreases. The TGA spectrum show that about 20 – 25 % of the initial mass loss occurs after heating to 100 ˚C which is due to entrapped water in the cavities.[10]

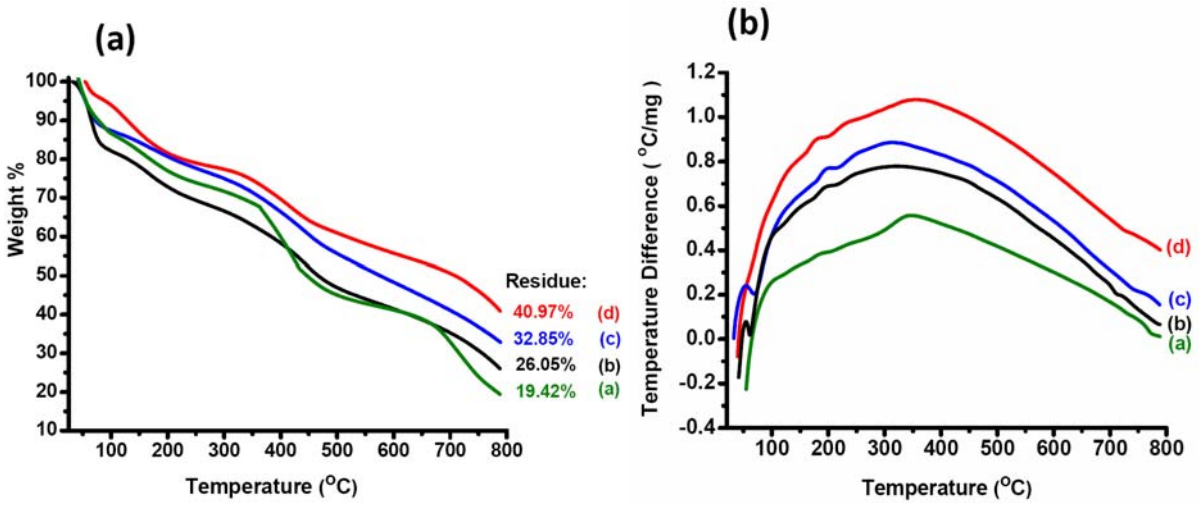

Figure S10. **(a)** TGA plots for freshly synthesized (G-dye - FeP)$_n$ MOF series (under N_2 , 10 °C /min) ,(a) (G - dye 50 wt % -FeP)$_n$ MOF , (b) (G - dye 25 wt % -FeP)$_n$ MOF,(c) (G - dye 10 wt % -FeP)$_n$ MOF, and (d) (G - dye 5 wt % -FeP)$_n$ MOF. **(b)** DTA plots for freshly synthesized (G-dye - FeP)$_n$ MOF series ,(a) (G - dye 50 wt % -FeP)$_n$ MOF , (b) (G - dye 25 wt % -FeP)$_n$ MOF,(c) (G - dye 10 wt % -FeP)$_n$ MOF, and (d) (G - dye 5 wt % -FeP)$_n$ MOF

S11. Evidences to prove the presence of Graphene sheet inside the framework

In order to prove the presence of graphene sheet inside the framework, the (G-dye 10 wt % -FeP)$_n$ MOF (rod-shaped) sample was dissolved in phosphate buffer followed by sonication (process (1)). After evaporating the solvent, the sample was washed with water and ethanol to remove iron-porphyrin and impurity from the G-dye. The collected sample was dried under vacuum (process (2)). Finally, the sample was dispersed in DMF and sonicated for 30 min (process (3)). The presence of r-GO sheets were revealed by optical microscopy, AFM, SEM and Raman spectroscopy (process (4)). Raman spectroscopy shows the D band (1347.5 cm^{-1}) and G band (1586.5 cm^{-1}) of the r-GO sheet (part d).[11]

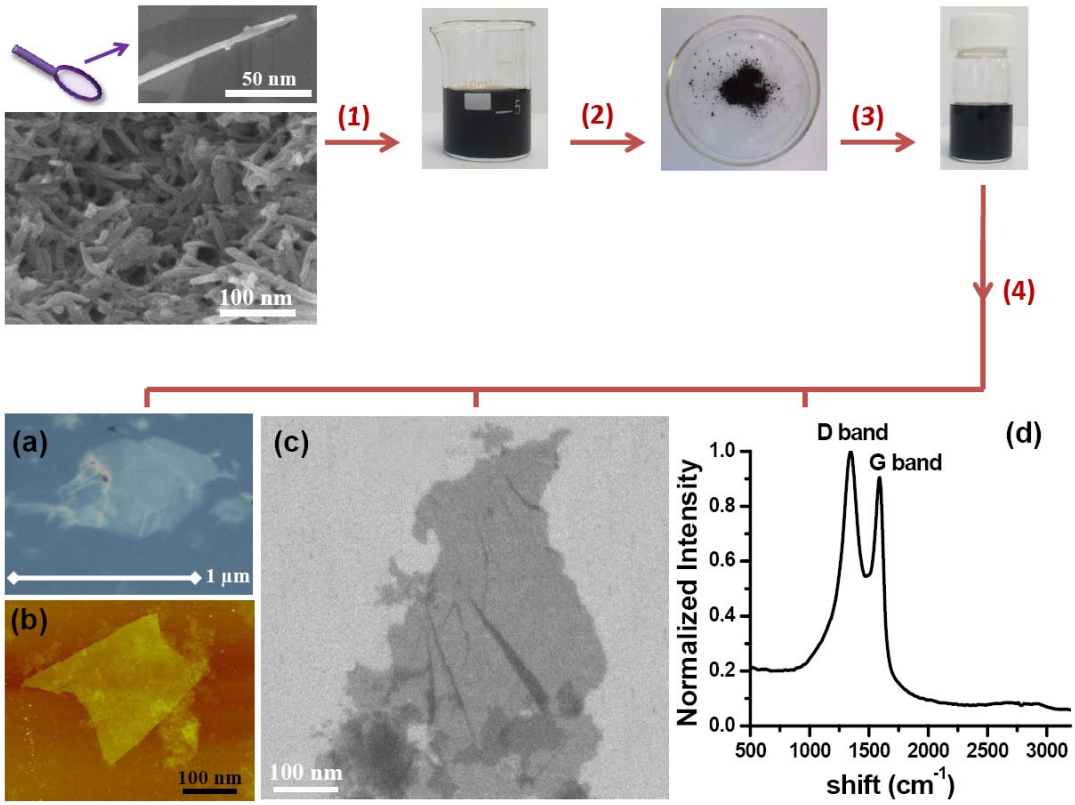

Figure S11. Schematic of the process flow to show how r-GO sheets were recovered from the rod-shaped (G-dye 10 wt % -FeP)$_n$ MOF after dissolving the iron-porphyrin MOF. *Process (1)* : After evaporating the solvent, the sample was washed with water and ethanol to remove iron- porphyrin and impurity from the G-dye. *Process (2):* The collected sample was dried under vacuum. *Process (3)*: The sample was dispersed in DMF and sonicated for 30 mins. *Process (4)*: It was checked by (a) optical microscopy , (b) AFM, (c) SEM and (d) Raman spectroscopy.

References:

(1) Jahan, M.; Bao, Q. L.; Yang, J. X.; Loh, K. P. *J. Am. Chem. Soc.* **2010**, *132*, 14487.

(2) Williams, J.; Adel, R.; Carlson, J.; Reynolds, G.; Borden, D.; Ford Jr, J. *J. Org. Chem* **1963**, *28*, 387.

(3) Jäger, M.; Eriksson, L.; Bergquist, J.; Johansson, O. *J. Org. Chem* **2007**, *72*, 10227.

(4) Si, Y.; Samulski, E. *Nano Lett.* **2008**, *8*, 1679.

(5) Lomeda, J.; Doyle, C.; Kosynkin, D.; Hwang, W.; Tour, J. *J. Am. Chem. Soc.* **2008**, *130*, 16201.

(6) Chung, H.; Barron, P. M.; Novotny, R. W.; Son, H. T.; Hu, C.; Choe, W. *Cryst. Growth Des.* **2009**, *9*, 3327.

(7) Robert L. Arechederra, Kateryna Artyushkova, Plamen Atanassov, and Shelley D. Minteer, *ACS Applied materials & interference,* **2010**, *2* , 3295.

(8) Shubin Yang, Xinliang Feng, Xinchen Wang, and Klaus Mullen , *Angew. Chem. Int. Ed.* **2011**, *50,* 5339.

(9) Cannon, C.; Butterworth, I. *Anal. Chem.* **1953,** *25*, 168.

(10) Zhao, X.; Lu, G.; Whittaker, A.; Millar, G.; Zhu, H. *J. Phys. Chem. B* **1997**, *101*, 6525.

(11) Dresselhaus, M. S.; Jorio, A.; Hofmann, M.; Dresselhaus, G.; Saito, R. *Nano Lett.* **2010**, *10*, 751.